

Achieving unidirectional propagation of twisted magnons in a magnetic nanodisk array

Zhixiong Li ¹, Xiansi Wang ², Xuejuan Liu,^{3,4} and Peng Yan ^{4,*}

¹*School of Physics, Central South University, Changsha 410083, China*

²*School of Physics and Electronics, Hunan University, Changsha 410082, China*

³*College of Physics and Engineering, Chengdu Normal University, Chengdu 611130, China*

⁴*School of Physics and State Key Laboratory of Electronic Thin Films and Integrated Devices, University of Electronic Science and Technology of China, Chengdu 610054, China*

 (Received 13 July 2023; revised 2 January 2024; accepted 4 January 2024; published 22 January 2024)

Twisted magnons (TMs) have great potential applications in communication and computing owing to the orbital angular momentum degree of freedom. Realizing the unidirectional propagation of TMs is the key to designing functional magnonic devices. Here we theoretically study the propagation of TMs in one-dimensional magnetic nanodisk arrays. By performing micromagnetic simulations, we find that the one-dimensional nanodisk array exhibits a few bands due to the collective excitations of TMs. A simple model of the exchange interaction is proposed to explain the emerging multiband structure, and theoretical results agree well with micromagnetic simulations. Interestingly, for a zigzag structure, the dispersion curves and propagation images of TMs show obvious nonreciprocity for a specific azimuthal quantum number (l), which originates from a geometric effect depending on the phase difference of TMs and the relative angle between two adjacent nanodisks. Utilizing this feature, one can conveniently realize the unidirectional propagation of TMs with arbitrary nonzero l . Our work provides important theoretical references for controlling the propagation of TMs.

DOI: [10.1103/PhysRevB.109.024428](https://doi.org/10.1103/PhysRevB.109.024428)

I. INTRODUCTION

Ever since the quantized orbital angular momentum (OAM) states were originally introduced in photonics [1–5], the peculiar twisted structure has been rapidly extended to a broad field of electronics [6–10], acoustics [11–15], neutronics [16–20], and spintronics [21–25]. In the magnetic system, the magnons (quantized quasiparticle of spin wave) carrying OAM are called twisted magnons (TMs) [21,22]. The research about the OAM states of magnons has attracted growing interest owing to both the fundamental interest and potential applications. By using the twisted phase structure of TMs as individual information channels, it is possible to realize the frequency-division multiplexing which can greatly enhance the communication capacity of magnons [25]. It has been proposed that the TMs can act as “magnetic tweezers” to drive the rotation of spin texture (such as skyrmion) [21]. Very recently, Wang *et al.* [26] showed that the magnonic frequency comb emerges in the nonlinear interaction between TMs and a magnetic vortex.

In magnonics or magnon spintronics [27–30], realizing the unidirectional information propagation based on spin waves (or magnons) is the key step for designing functional devices. So far, the unidirectional magnons have been demonstrated by various mechanisms [31], such as magneto-dipolar interaction (Damon-Eshbach surface modes) [32,33], Dzyaloshinskii-Moriya interactions [34,35], topological bands (magnon edge state) [36–38], etc. However, these works are based

on conventional magnons, and few studies have discussed the unidirectional propagation of TMs, which are vital to TM-based devices. Generally speaking, TMs only exist in magnetic nanocylinders. On the one hand, Jiang *et al.* [21] and Jia *et al.* [22] have theoretically studied the spectrum of TMs in a single magnetic nanocylinder with a small aspect ratio (radius relative to height). In such a configuration, it is, however, difficult to excite the TMs with a specific l because of the multiband structure. On the other hand, although the intrinsic dynamics of TMs in a single magnetic nanocylinder with a big aspect ratio (also known as a nanodisk) has been investigated [25], the collective dynamics of TMs in nanodisk arrays is rarely explored. The magnetic nanodisk array is an ideal platform for studying the collective propagation of TMs for the following reasons.

(i) The desired lattice structure based on magnetic nanodisks can be fabricated within the reach of current experimental techniques, for example, electron-beam lithography [39–41].

(ii) It is convenient to excite TMs with arbitrary l in nanodisk arrays by means of the so-called spin-to-orbital angular momentum conversion mechanism [25].

(iii) For two- or three-dimensional nanodisk lattices, one may realize the chiral propagation of TMs with topological features. It is thus naturally expected that the collective excitations of TMs in nanodisks array can exhibit abundant physics (unidirectional propagation, for instance), which should provide important theoretical references for designing functional magnonic devices.

In this work, we study the collective dynamics of TMs in one-dimensional magnetic nanodisk arrays. For a straight

*Corresponding author: yan@uestc.edu.cn

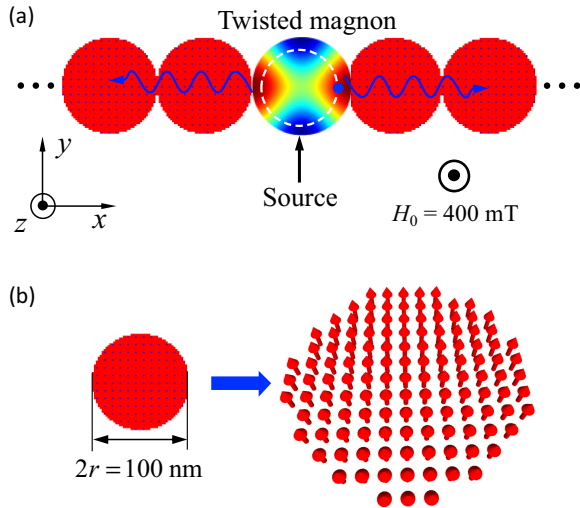


FIG. 1. (a) The illustration of a straight one-dimensional lattice containing 101 magnetic nanodisks. A uniform static magnetic field is applied along the z axis to perpendicularly magnetize the magnetic moments. The TMs are excited at the center disk, marked by a black arrow. (b) Zoomed-in details of one nanodisk. The red arrows denote the local magnetization.

lattice, the system supports a few symmetric magnon bands describing different collective excitation modes of TMs. A simple exchange model is proposed to explain the emergence of the multiband structure. Interestingly, for the zigzag structure, the TM dispersion relations can exhibit visible nonreciprocity. These asymmetric bands are explained by a geometric effect: When the phase difference of TMs does not match the geometric angle (θ) [see Fig. 3(b)], the nonreciprocity occurs. It allows us to realize unidirectional propagation of TMs for any nonzero l by tuning θ . In addition, we find that the propagation direction of TMs can be conveniently tuned by changing the sign of l or the position of the excitation field. Our results provide a simple and effective method to control the propagation of TMs which should greatly promote the development of twisted magnonics.

The paper is organized as follows. In Sec. II, we present both micromagnetic simulations and theoretical analyses for TM band structures in straight one-dimensional nanodisk lattices. Section III focuses on the unidirectional propagation of TMs in a zigzag nanodisk array. Discussion and conclusions are presented in Sec. IV.

II. THE TM BAND STRUCTURES FOR STRAIGHT LATTICE

We consider a straight one-dimensional lattice consisting of 101 identical magnetic nanodisks with radius $r = 50$ nm and thickness $d = 2$ nm, as shown in Fig. 1. The distance between nearest-neighboring nanodisks is $2r$, which indicates that the TMs can interact with each other through the exchange interaction. The material parameters of yttrium iron garnet are used [25]: The saturation magnetization $M_s = 1.92 \times 10^5$ A m $^{-1}$, the exchange stiffness $A = 3.1 \times 10^{-12}$ J m $^{-1}$, and the Gilbert damping constant $\alpha = 10^{-3}$. The magnetic moments are perpendicularly magnetized by

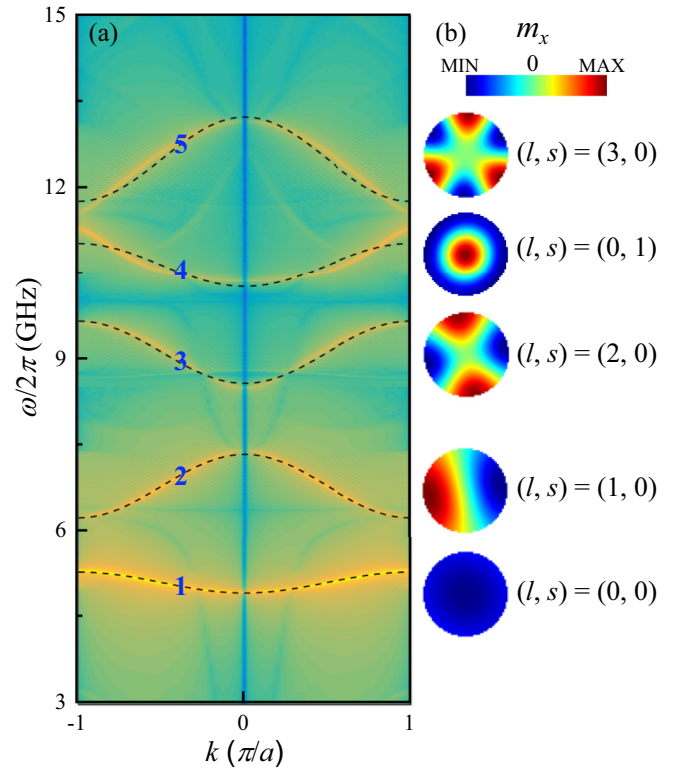


FIG. 2. (a) Dispersion relations of TMs for the structure in Fig. 1(a). The background color and dashed black lines represent the simulation results and analytical formulas, respectively. (b) The spatial distribution of FFT intensity for different TM modes which correspond to the five bands emerging in panel (a). Here s denotes the radial quantum number which gives the number of nodes along the radial direction.

the external magnetic field $H_0 = 400$ mT. The cell size is set to be $2 \times 2 \times 2$ nm 3 . The micromagnetic software package MUMAX3 [42] is used to simulate the magnetization dynamics. To excite the collective oscillation of TMs, we apply a sinc-function magnetic field:

$$\mathbf{H}(t) = H_1 \frac{\sin[2\pi f_0(t - t_0)]}{2\pi f_0(t - t_0)} [\cos(l\phi), \sin(l\phi), 0], \quad (1)$$

with $H_1 = 40$ mT, $f_0 = 15$ GHz (cutoff frequency), and $t_0 = 1$ ns, confined to the disk located at the center of the lattice, as labeled by the black arrow in Fig. 1(a). Here ϕ is the polar angle. The spatiotemporal profiles of magnetizations in all nanodisks are recorded every 20 ps and the total simulation time is 200 ns.

The dispersion relation of TMs is obtained by calculating the spatiotemporal fast Fourier transformation (FFT) of the averaged (over the whole disk) magnetization x component (m_x) (or y component). For every azimuthal (OAM) quantum number l , we can calculate the spectrum. To get the full band structure, we sum the spectra for $l = 0, 1, 2$. Figure 2 shows the results, from which we can clearly see that the system exhibits five separate dispersion curves below 15 GHz, as marked by the arabic numbers 1–5 shown in blue. Besides, by analyzing the spatial distribution of the FFT intensity for these bands, we can identify five different TM modes, as

shown in Fig. 2(b). Interestingly, we find that the signs of the group velocity are opposite when l is even (bands 1, 3, and 4) and odd (bands 2 and 5) for the same wave vector k . Moreover, there are some additional inconspicuous bands in Fig. 2 which may come from the hybridization between different TMs because the frequencies of these states are very close.

To explain the emerging multiband structure of TMs, we propose a theoretical model which is similar to the framework of the massless Thiele's equation [43]. Here the dynamics of TMs can be described by an analogous Thiele's equation based on the following facts. At first, due to the distinctive mode profile of TMs (see Fig. 2), it is reasonable to use a wave-packet description. Then we consider the position of the peak (or trough) to represent the TMs in nanodisks because of the circular symmetry, as denoted by the blue ball in Fig. 1(a) [here $(l, s) = (2, 0)$]. At last, we envision that the steady-state magnetization of the nanodisk only depends on the position of TMs.

Assuming the displacement vector of TMs from the disk center as $\mathbf{U}_j = (u_j, v_j)$ defined by the position of the amplitude maximum of TMs with a constant phase in the j th nanodisk, we obtain the dynamic equation characterizing TMs as

$$G\dot{z} \frac{d\mathbf{U}_j}{dt} + \mathbf{F}_j = 0, \quad (2)$$

where G is a gyroscopic coefficient. The conservative force can be expressed as $\mathbf{F}_j = -\partial W / \partial \mathbf{U}_j$. Here W denotes the total potential energy:

$$W = \sum_j K \mathbf{U}_j^2 / 2 + W_d + W_z + W_e. \quad (3)$$

The first term on the right-hand side of Eq. (3) originates from the confinement of the disk boundary, while the terms W_d , W_z , and W_e represent the potential energy from magnetostatic, Zeeman, and exchange interactions, respectively.

Then we consider the excitation of TMs, i.e., $\mathbf{m} = (m_x, m_y, 1)$, with $m_x^2 + m_y^2 \ll 1$, and with \mathbf{m} being the unit vector of the local magnetic moment. It is straightforward that the Zeeman energy $-\mu_0 M_s \int H_0 \hat{z} \cdot \mathbf{m} d\mathbf{r} = -N\mu_0 M_s H_0$ is a constant. Here, μ_0 is vacuum permeability and N is the number of magnetic moments. Moreover, the magnetostatic energy is approximately considered as a constant, which originates from the fact that the change of magnetostatic energy is much smaller than the exchange energy when TMs are excited. On the one hand, we have performed the dispersion relation of TMs when magnetostatic energy is excluded (TMs are coupled only by exchange interaction). In this case, we find that the shapes of the band structures are almost the same as those when considering dipolar interaction. The only change is that the position of the band center shifts towards higher frequency. On the other hand, we have identified that the dipolar interaction cannot efficiently couple TMs when we artificially leave a physical gap between nearest-neighboring nanodisks even as short as 1 nm. We therefore conclude that the exchange interaction dominates the collective dynamics of TMs in a nanodisk array.

The exchange coupling between adjacent disks is mediated through the magnetic moments in the vicinity of the contact

TABLE I. The fitting parameters for different TM modes.

	TM mode (l, s)				
	(0, 0)	(1, 0)	(2, 0)	(0, 1)	(3, 0)
$C_1/2\pi$ (GHz)	5.11	6.80	9.13	10.66	12.51
$C_2/2\pi$ (GHz)	-0.18	0.55	-0.54	-0.38	0.73

points. Different \mathbf{U}_j will generate different magnitudes of magnetization oscillation near the edge. A minimum model of the coupling between adjacent disks is thus the isotropic exchange term expressed as $I\mathbf{U}_j \cdot \mathbf{U}_k$. We therefore obtain the total exchange energy

$$W_e = \sum_{k \in \langle j \rangle} I \mathbf{U}_j \cdot \mathbf{U}_k, \quad (4)$$

with I being the isotropic coupling coefficient. It is noted that the coupling coefficient I depends on the integral indexes l and s of the TM modes. Then the total potential energy becomes the following:

$$W = W_0 + \sum_j K \mathbf{U}_j^2 / 2 + \sum_{k \in \langle j \rangle} I \mathbf{U}_j \cdot \mathbf{U}_k, \quad (5)$$

where $W_0 = W_d + W_z$ denotes the constant term of energy, and $\langle j \rangle$ is the set of nearest neighbors of j .

Substituting Eq. (5) into Eq. (2) and assuming $\psi_j = u_j + iv_j$, we obtain the eigenequation

$$\frac{d\psi_j}{dt} + iC_1\psi_j + iC_2(\psi_{j-1} + \psi_{j+1}) = 0, \quad (6)$$

with parameters $C_1 = K/G$ and $C_2 = I/G$. Then we consider the plane-wave expansion of $\psi_j = \phi \exp(-i\omega t) \exp[i(\mathbf{k} \cdot \mathbf{a})]$, where \mathbf{k} is the wave vector, $\mathbf{a} = a\hat{x}$ is the basis vector with $a = 100$ nm representing the lattice constant. We thus obtain the following dispersion relation of TMs:

$$\omega = C_1 + 2C_2 \cos(\mathbf{k} \cdot \mathbf{a}). \quad (7)$$

Then we use the formula (7) to fit the dispersion curves of TMs obtained from micromagnetic simulation. The dashed black lines in Fig. 2 show the best fit of the numerical data, from which we can clearly see that the theoretical curves agree well with simulations for small values of l or s (bands 1, 2, and 3). However, for larger values of l or s (bands 4 and 5), there exists an obvious discrepancy between theoretical values and micromagnetic results, which may come from the fact that the form of exchange energy (4) is too simple to accurately describe the interaction between TMs with high values of l (or s). The fitting parameters C_1 and C_2 for different values of l or s are summarized in Table I. Overall, C_1 and C_2 are sensitive to l and s : (i) the parameter C_1 is always positive, while C_2 is negative (positive) when l takes an even (odd) number, and (ii) with the increase of l (s) for fixed s (l), the magnitude of C_1 and C_2 increases. The sign and magnitude of C_2 can be understood by using the theoretical model (see Appendix A for details).

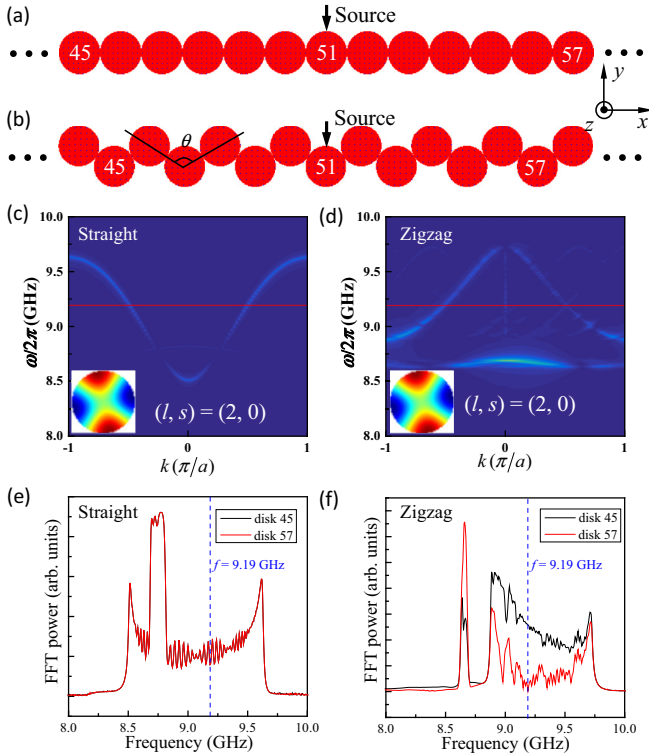


FIG. 3. Schematic diagrams of (a) straight and (b) zigzag one-dimensional nanodisk arrays. Black arrows denote the disks where the excitation fields are applied. The angle $\theta = 2\pi/3$ (formed by lines connecting the centers of two adjacent disks) describes the geometric shape of the zigzag structure. The band structures for (c) straight and (d) zigzag structures with $(l, s) = (2, 0)$. The red lines represent the frequency $\omega/2\pi = 9.19$ GHz. The temporal Fourier spectra of the magnetization oscillation at disks 45 and 57 [as marked in panels 3(a) and 3(b)] for (e) straight and (f) zigzag lattices.

III. UNIDIRECTIONAL PROPAGATION OF TMs

Next, we discuss the propagation characteristics of TMs in a zigzag structure, as shown in Fig. 3(b). By changing the value of θ , one can tune the geometric shape of the lattice. We first choose $\theta = 2\pi/3$ as an example. Interestingly, in this case, the dispersion relations of TMs show obvious nonreciprocity for $l = 1$ and $l = 2$ [see Figs. 3 and 4], which is in sharp contrast to the straight structure. We focus on this feature in this section.

Figures 3(c) and 3(d) show the band structures of TM with $(l, s) = (2, 0)$ for straight and zigzag lattices, respectively. Here the excitation fields with the form of Eq. (1) are applied to disk 51 (the center disk). One can clearly see that the FFT strength of dispersion curves are symmetric for $+k$ and $-k$ in the straight lattice, while they shows a visible asymmetric feature for the zigzag case. Besides, we plot the spectra of the magnetization (m_x) oscillation at disks 45 and 57 [as marked in Figs. 3(a) and 3(b)], as shown in Figs. 3(e) and 3(f), from which one can identify again the existence of nonreciprocity for TM propagation in the zigzag lattice. Moreover, the TMs with $(l, s) = (1, 0)$ also exhibit similar behaviors, as plotted in Fig. 4. The band structures [Figs. 4(a) and 4(b)] and the disk

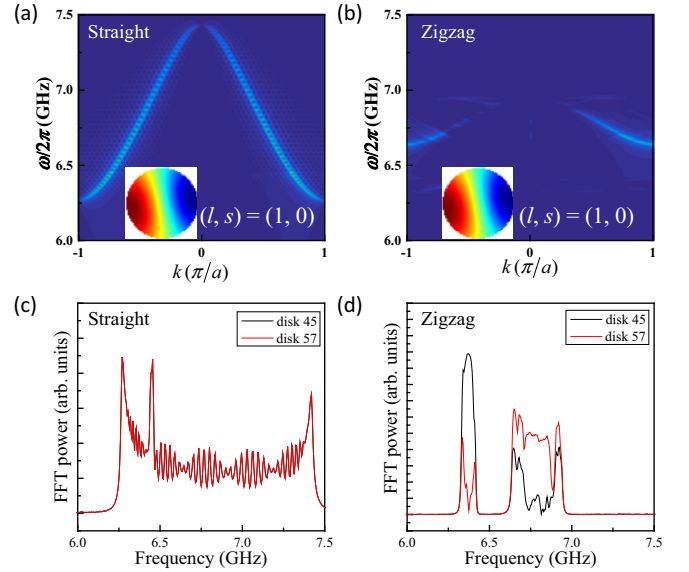


FIG. 4. The band structures for (a) straight lattice and (b) zigzag lattice with $(l, s) = (1, 0)$. The corresponding spectra of the magnetization oscillation at disks 45 and 57 for (c) straight lattice and (d) zigzag lattice.

spectra [Figs. 4(c) and 4(d)] clearly show that the propagation of TMs [$(l, s) = (1, 0)$] is nonreciprocal (reciprocal) for the zigzag (straight) shape. However, for $l = 0$ and $l = 3$, the dispersion relations are symmetric in both zigzag and straight lattices (see Appendix B for details). Besides, we also checked that the TMs exhibit similar behaviors (reciprocal and nonreciprocal propagations) when dipolar interaction is removed (not shown here). It is worth noting that the difference of the FFT power intensity of the unidirectional TM dispersion relation [see Figs. 3(d) and 4(b)] is not very significant, which may be for the following reasons. On the one hand, the number (101) of nanodisks is still too small to show the unidirectional propagation of TMs. On the other hand, the damping coefficient adopted is too small (10^{-3}), which allows a finite extension of the forbidden TM modes.

To further visualize the nonreciprocal propagation of TMs, we choose one representative frequency: $f_1 = 9.19$ GHz for $(l, s) = (2, 0)$, as marked by red lines in Fig. 3. We then simulate the dynamics of TMs by the excitation field

$$\mathbf{B}(t) = B_0 \sin(2\pi f_1 t) [\cos(l\phi), \sin(l\phi), 0], \quad (8)$$

with $B_0 = 1$ mT applied at the center disk, indicated by the black arrows in Fig. 5. Figure 5(b) shows the propagation of TMs in the zigzag structure, from which one can clearly observe the unidirectional propagation of TMs. For comparison, we also plot the propagation images of TMs in the straight lattice, as shown in Fig. 5(a), which shows a symmetric spread. Interestingly, we find that for the zigzag structure, the propagation direction of TMs can be reversed by changing the sign of l [see Fig. 5(c)] or the position of the excitation field [see Fig. 5(d)].

The physical mechanism of the symmetric and asymmetric TM dispersion relations can be explained as a geometric effect. For $l = 0$, because the phase structure of TMs is symmetric along any radius direction (see Fig. 2), the propagation

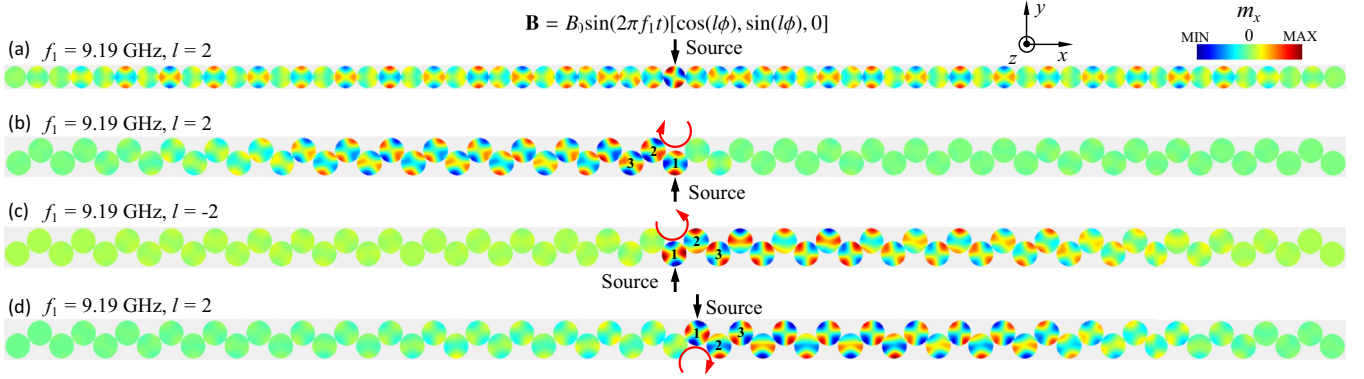


FIG. 5. The spatial distribution of TM intensity in one-dimensional (a) straight and [(b)–(d)] zigzag nanodisk arrays. Here $l = 2$ in panels (a), (b), and (d), and $l = -2$ in panel (c). Black arrows denote the disk where the driving field \mathbf{B} is applied. The simulation time $t = 10$ ns. The red arrows represent the rotation direction of the TM in the source disk and arabic numbers 1–3 are marked for better illustration.

of TMs is thus symmetric for both straight and zigzag lattices, as shown in Fig. 7. It is noteworthy that this conclusion always holds for any θ (here the condition $\pi/3 < \theta \leq \pi$ should be satisfied to guarantee that there is no overlap between neighboring nanodisks. If $\theta = \pi/3$, each disk is tangential to the four surrounding disks and the system is no longer a simple one-dimensional structure). For $l \neq 0$, we define $\beta = \pi/l$ to represent the angle between the nearest-neighbor azimuthal nodes of the TM. At first, we must stress the fact that the TM can spread to an adjacent disk only when the contact point is not at the node of the TM. Considering that the TM is excited in a nanodisk, when the left contact point is (not) located at the node of the TM, the right contact point is also (not) located at the node, if θ is an integer multiple of β . In this case, the dispersion relation is symmetric. However, if θ is not an integer multiple of β , the two contact points of the nanodisk cannot be located at the nodes of the TM simultaneously, the band structure of the TM thus becomes asymmetric. These conclusions can be used to explain our results. On the one hand, for the straight lattice, i.e., $\theta = \pi$, no matter what value l takes, θ is always an integer multiple of β . Therefore, the dispersion relations for all l are reciprocal (see

Fig. 2). On the other hand, for the zigzag structure considered in our paper, i.e., $\theta = 2\pi/3$, the situation is different. When $l = 1$ and $\beta = \pi$, then $\theta = 2\pi/3$ is not an integer multiple of β . Naturally, the dispersion relation is asymmetrical for $(l, s) = (1, 0)$ [see Fig. 4]. We can do a similar analysis for $l = 2$: In this case, $\beta = \pi/2$, and again, θ is not an integer multiple of β , the dispersion relation is thus asymmetric for $(l, s) = (2, 0)$ [see Fig. 3]. However, when $l = 3$ and $\beta = \pi/3$, we have $\theta = 2\beta$, and therefore, the band structure is reciprocal for $(l, s) = (3, 0)$ [see Figs. 7(i) and 7(l)]. Here the spectra show a little nonreciprocity which originates from the fact that the software MUMAX3 is based on the finite difference method, and the position of contact is thus not a strict point. At last, it is worth noting that the propagation direction of the unidirectional TMs depends on both the sign of l and the position of the excitation field [we use $P = 1$ ($P = -1$) to denote the excitation field located at the lower (upper) disks]. Concretely, when $\text{sgn}(l)\text{sgn}(P) = 1$ (or -1), the TMs propagate leftward (or rightward).

The propagation direction of nonreciprocal TMs can be explained as a “ratcheting effect,” i.e., the energy (or oscillation) propagates along the direction of TM rotation. For $l = 2$ [see Fig. 5(b)], the rotation direction of the TM in the source disk (marked by arabic number 1) is clockwise, the left contact disk (marked by arabic number 2), therefore, can receive the information of magnetization oscillation, while the right contact disk cannot. Notably, here the rotating TMs can be acting as gears, and for the external meshing system, the adjacent gears rotate in opposite directions. Thus, the rotation direction of the TM in disk 2 changes to anticlockwise, and naturally, the oscillation can spread to disk 3 (the rotation direction of the TM turns into clockwise again). As a result, the TMs exhibit unidirectional propagation to the left. For $l = -2$ and the case where the excitation source is located on the lower disk [see Figs. 5(c) and 5(d)], we can do a similar analysis.

Based on the above analysis, we can easily infer that when one contact point is located at the node, if the other contact point is located at the peak (or trough), the nonreciprocity of TMs reach the maximum. In this case, $\theta = (2n + 1)\pi/2l$, with $n = 0, 1, 2, 3 \dots$ (note the condition $\pi/3 < \theta \leq \pi$ should be satisfied simultaneously). We, therefore, can

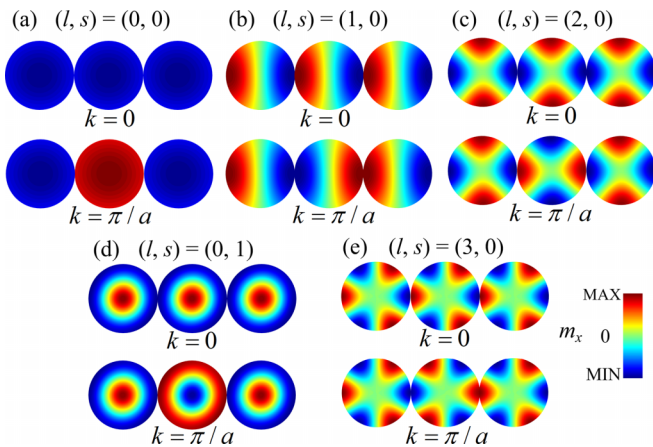


FIG. 6. The illustration of the collective oscillation distribution in the disk array for TM modes (a) $(l, s) = (0, 0)$, (b) $(1, 0)$, (c) $(2, 0)$, (d) $(0, 1)$, and (e) $(3, 0)$ when $k = 0$ and $k = \pi/a$.

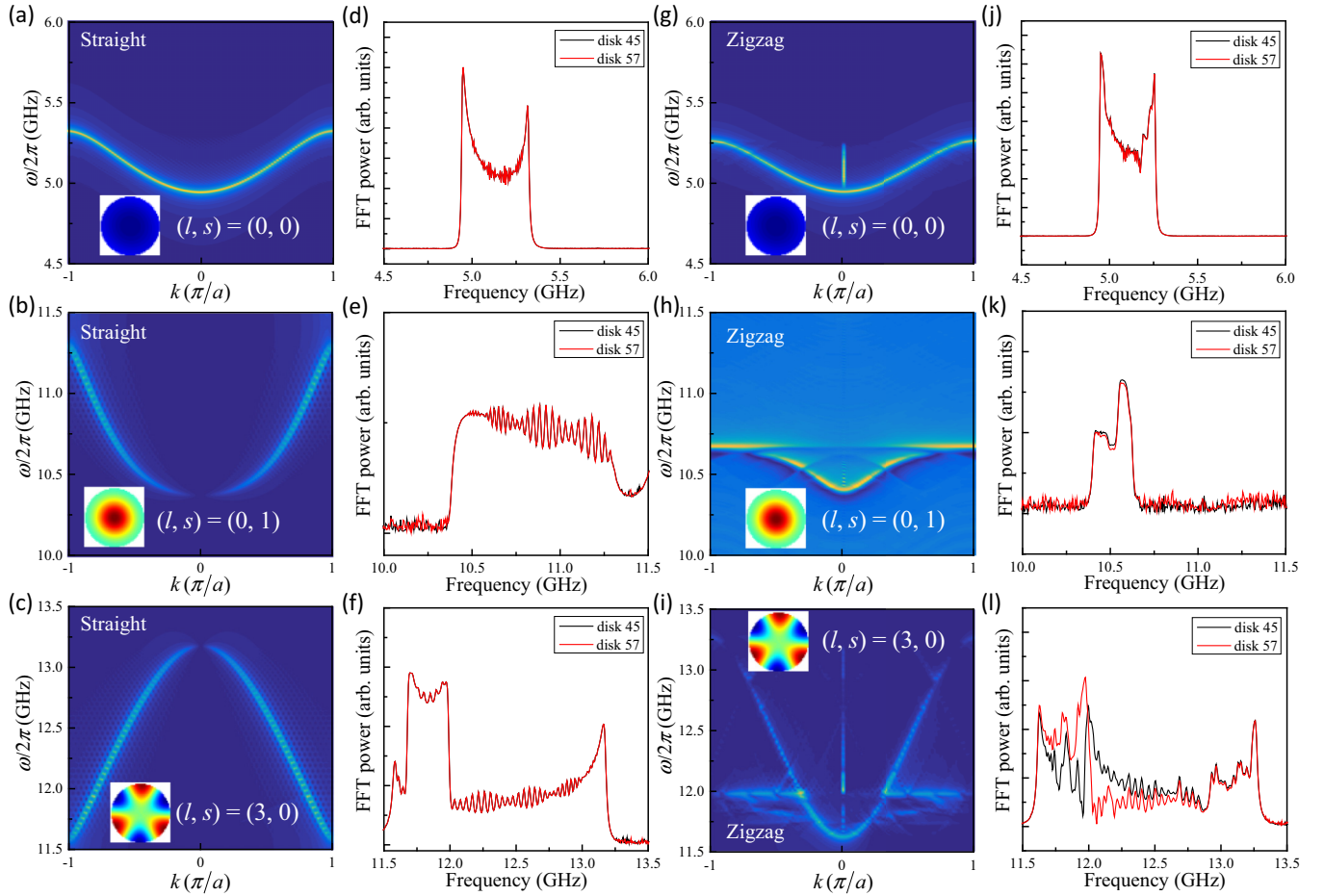


FIG. 7. The band structures for [(a)–(c)] straight and [(g)–(i)] zigzag lattices with different values of l or s as marked in the images. The corresponding spectra of the magnetization oscillation at disks 45 and 57 for [(d)–(f)] straight and [(j)–(l)] zigzag lattices.

realize the unidirectional propagation of TMs for any nonzero l by tuning θ .

IV. DISCUSSION AND CONCLUSION

The research about the twisted magnonics is still in the very initial stage, and a lot of questions need to be answered and new phenomena need to be discovered. For example, by constructing the Su-Schrieffer-Heeger [44] and Haldane [45] models based on magnetic nanodisks, we can realize the topological edge states of TMs, which may have great potential for designing topologically protected high-capacity communication devices. Besides, the interaction between TMs and various spin textures (for example, skyrmion, vortex, and domain wall, etc.) also deserves careful investigation, which may lead to peculiar phenomena, for example, magnetic frequency combs [26].

To conclude, we have studied the collective excitations of TMs in one-dimensional magnetic nanodisk arrays. For a straight lattice, by performing micromagnetic simulations, we identified multiple symmetric bands which characterize different collective modes of TMs. A theoretical model was proposed to explain the band structure and the results agree well with simulations. For the zigzag structure, we found that the TM dispersion relations for $l = 1$ and $l = 2$ show

obvious nonreciprocity, which do not happen for $l = 0$ and $l = 3$. The propagation characteristics (reciprocal or nonreciprocal) of these bands result from a geometric effect: When θ is (not) an integer multiple of β ($= \pi/l$), the dispersion relation is symmetric (asymmetric). Utilizing this principle, we can achieve unidirectional propagation of TMs with any nonzero l . Our work provides a simple and effective method to manipulate the propagation of TMs, which should be helpful for designing useful TM devices.

ACKNOWLEDGMENTS

We thank Z. Wang and H. Y. Yuan for helpful discussions. This work was supported by the National Key Research and Development Program under Contract No. 2022YFA1402802 and the National Natural Science Foundation of China (NSFC) (Grants No. 12074057 and No. 12374103). Z.-X.L. acknowledges financial support from the NSFC (Grant No. 11904048) and the Natural Science Foundation of Hunan Province of China (Grant No. 2023JJ40694). X.S.W. was supported by the NSFC (Grants No. 12174093 and No. 11804045) and the Fundamental Research Funds for the Central Universities. X.L. acknowledges support from the Talent Introduction Program of Chengdu Normal University under Grant No. YJRC2021-14.

APPENDIX A: THE DISCUSSION ABOUT THE SIGN AND MAGNITUDE OF PARAMETER C_2

From Eq. (7), we know that the parameter C_2 determines the shape of the band structures. On the one hand, for TM mode $(l, s) = (0, 0)$, when wave vector $k = 0$ ($k = \pi/a$), the adjacent TMs oscillate in-phase (out-of-phase), as shown in Fig. 6(a). The exchange energy of in-phase oscillation is therefore lower than the out-of-phase oscillation, and the band exhibits a downward concave shape, i.e., the sign of C_2 is negative. We can do a similar analysis on the TM modes $(l, s) = (2, 0)$ and $(0, 1)$; please see Figs. 6(c) and 6(d). However, the situations are different for $(l, s) = (1, 0)$ and $(3, 0)$, the magnetic moments near the contact point oscillate out-of-phase (in-phase) for $k = 0$ ($k = \pi/a$), as shown in Figs. 6(b) and 6(e). The exchange energy for $k = 0$ is therefore higher than that for $k = \pi/a$, and the dispersion relation shows a upward convex shape, i.e., the sign of C_2 is positive. On the other hand, as discussed above, a large value of \mathbf{U}_j will lead to a strong exchange coupling. The position of the amplitude maximum of TMs is close to the center (boundary) of the disk for TM modes $(l, s) = (0, 0)$ and $(0, 1)$ [$(l, s) = (1, 0)$, $(2, 0)$, and $(3, 0)$], the values of I (or I/G , G is a positive coefficient) for $(l, s) = (0, 0)$ and $(0, 1)$ thus are smaller than those for $(l, s) = (1, 0)$, $(2, 0)$, and $(3, 0)$. Besides, comparing TM modes $(l, s) = (0, 0)$ and $(0, 1)$, we can see that the oscillation of the magnetic moment

at the boundary (or contact point) for mode $(l, s) = (0, 1)$ is stronger than that for mode $(l, s) = (0, 0)$. As a result, the coupling coefficient I for mode $(l, s) = (0, 1)$ has a larger value. Moreover, for TM modes $(l, s) = (1, 0)$, $(2, 0)$, and $(3, 0)$, it can be seen that the position of the amplitude maximum of the TM for mode $(l, s) = (3, 0)$ is more localized to the disk boundary compared to TM modes $(l, s) = (1, 0)$ and $(2, 0)$; therefore, the magnitude of I for mode $(l, s) = (3, 0)$ is the largest one.

APPENDIX B: THE BAND STRUCTURES FOR $l = 0$ AND $l = 3$

Figure 7 plots the dispersion relation and disk spectra for $l = 0$ and $l = 3$ with the help of micromagnetic simulations. One can clearly see that the propagations of TMs are absolutely symmetric [see Figs. 7(a)–7(f)] in a straight lattice. For the zigzag lattice, the bands and spectra show symmetric characteristics for $l = 0$ [see Figs. 7(g), 7(h), 7(j), and 7(k)]. There exists a little nonreciprocity for $l = 3$ [see Figs. 7(i) and 7(l)], which comes from the calculation errors because of the finite difference method (also see related discussions in the main text). We thus conclude that the propagations of TMs are reciprocal for $l = 0$ and $l = 3$ in both straight and zigzag structures.

-
- [1] L. Allen, M. W. Beijersbergen, R. J. C. Spreeuw, and J. P. Woerdman, Orbital angular momentum of light and the transformation of Laguerre-Gaussian laser modes, *Phys. Rev. A* **45**, 8185 (1992).
- [2] G. Molina-Terriza, J. P. Torres, and L. Torner, Twisted photons, *Nat. Phys.* **3**, 305 (2007).
- [3] M. J. Padgett, Orbital angular momentum 25 years on, *Opt. Express* **25**, 11265 (2017).
- [4] Z. Ji, W. Liu, S. Krylyuk, X. Fan, Z. Zhang, A. Pan, L. Feng, A. Davydov, and R. Agarwal, Photocurrent detection of the orbital angular momentum of light, *Science* **368**, 763 (2020).
- [5] S. Franke-Arnold, 30 years of orbital angular momentum of light, *Nat. Rev. Phys.* **4**, 361 (2022).
- [6] M. Uchida and A. Tonomura, Generation of electron beams carrying orbital angular momentum, *Nature (London)* **464**, 737 (2010).
- [7] J. Verbeeck, H. Tian, and P. Schattschneider, Production and application of electron vortex beams, *Nature (London)* **467**, 301 (2010).
- [8] B. J. McMorran, A. Agrawal, I. M. Anderson, A. A. Herzing, H. J. Lezec, J. J. McClelland, and J. Unguris, Electron vortex beams with high quanta of orbital angular momentum, *Science* **331**, 192 (2011).
- [9] A. J. Silenko, P. Zhang, and L. Zou, Manipulating twisted electron beams, *Phys. Rev. Lett.* **119**, 243903 (2017).
- [10] S. M. Lloyd, M. Babiker, G. Thirunavukkarasu, and J. Yuan, Electron vortices: Beams with orbital angular momentum, *Rev. Mod. Phys.* **89**, 035004 (2017).
- [11] P. Z. Dashti, F. Alhassen, and H. P. Lee, Observation of orbital angular momentum transfer between acoustic and optical vortices in optical fiber, *Phys. Rev. Lett.* **96**, 043604 (2006).
- [12] A. Anhäuser, R. Wunenburger, and E. Brasselet, Acoustic rotational manipulation using orbital angular momentum transfer, *Phys. Rev. Lett.* **109**, 034301 (2012).
- [13] D. Baresch, J.-L. Thomas, and R. Marchiano, Orbital angular momentum transfer to stably trapped elastic particles in acoustical vortex beams, *Phys. Rev. Lett.* **121**, 074301 (2018).
- [14] A. Marzo, M. Caleap, and B. W. Drinkwater, Acoustic virtual vortices with tunable orbital angular momentum for trapping of Mie particles, *Phys. Rev. Lett.* **120**, 044301 (2018).
- [15] K. Y. Bliokh and F. Nori, Spin and orbital angular momenta of acoustic beams, *Phys. Rev. B* **99**, 174310 (2019).
- [16] C. W. Clark, R. Barankov, M. G. Huber, M. Arif, D. G. Cory, and D. A. Pushin, Controlling neutron orbital angular momentum, *Nature (London)* **525**, 504 (2015).
- [17] R. L. Cappelletti, T. Jach, and J. Vinson, Intrinsic orbital angular momentum states of neutrons, *Phys. Rev. Lett.* **120**, 090402 (2018).
- [18] H. Larocque, I. Kaminer, V. Grillo, R. W. Boyd, and E. Karimi, Twisting neutrons may reveal their internal structure, *Nat. Phys.* **14**, 1 (2018).
- [19] A. V. Afanasev, D. V. Karlovets, and V. G. Serbo, Schwinger scattering of twisted neutrons by nuclei, *Phys. Rev. C* **100**, 051601(R) (2019).
- [20] J. A. Sherwin, Scattering of slow twisted neutrons by ortho- and parahydrogen, *Phys. Lett. A* **437**, 128102 (2022).
- [21] Y. Jiang, H. Y. Yuan, Z.-X. Li, Z. Wang, H. W. Zhang, Y. Cao, and P. Yan, Twisted magnon as a magnetic tweezer, *Phys. Rev. Lett.* **124**, 217204 (2020).
- [22] C. Jia, D. Ma, A. F. Schäffer, and J. Berakdar, Twisted magnon beams carrying orbital angular momentum, *Nat. Commun.* **10**, 2077 (2019).

- [23] M. Chen, A. F. Schäffer, J. Berakdar, and C. Jia, Generation, electric detection, and orbital-angular momentum tunneling of twisted magnons, *Appl. Phys. Lett.* **116**, 172403 (2020).
- [24] C. Jia, D. Ma, A. F. Schäffer, and J. Berakdar, Twisting and tweezing the spin wave: On vortices, skyrmions, helical waves, and the magnonic spiral phase plate, *J. Opt.* **21**, 124001 (2019).
- [25] Z.-X. Li, Z. Wang, Y. Cao, and P. Yan, Generation of twisted magnons via spin-to-orbital angular momentum conversion, *Phys. Rev. B* **105**, 174433 (2022).
- [26] Z. Wang, H. Y. Yuan, Y. Cao, and P. Yan, Twisted magnon frequency comb and Penrose superradiance, *Phys. Rev. Lett.* **129**, 107203 (2022).
- [27] V. V. Kruglyak, S. O. Demokritov, and D. Grundler, Magnonics, *J. Phys. D: Appl. Phys.* **43**, 264001 (2010).
- [28] A. A. Serga, A. V. Chumak, and B. Hillebrands, YIG magnonics, *J. Phys. D: Appl. Phys.* **43**, 264002 (2010).
- [29] B. Lenk, H. Ulrichs, F. Garbs, and M. Münzenberg, The building blocks of magnonics, *Phys. Rep.* **507**, 107 (2011).
- [30] A. V. Chumak, V. I. Vasyuchka, A. A. Serga, and B. Hillebrands, Magnon spintronics, *Nat. Phys.* **11**, 453 (2015).
- [31] J. Chen, H. Yu, and G. Gubbiotti, Unidirectional spin-wave propagation and devices, *J. Phys. D: Appl. Phys.* **55**, 123001 (2022).
- [32] K. L. Wong, L. Bi, M. Bao, Q. Wen, J. P. Chatelon, Y.-T. Lin, C. A. Ross, H. Zhang, and K. L. Wang, Unidirectional propagation of magnetostatic surface spin waves at a magnetic film surface, *Appl. Phys. Lett.* **105**, 232403 (2014).
- [33] M. Mohseni, R. Verba, T. Brächer, Q. Wang, D. A. Bozhko, B. Hillebrands, and P. Pirro, Backscattering immunity of dipole-exchange magnetostatic surface spin waves, *Phys. Rev. Lett.* **122**, 197201 (2019).
- [34] F. Ma and Y. Zhou, Interfacial Dzyaloshinskii-Moriya interaction induced nonreciprocity of spin waves in magnonic waveguides, *RSC Adv.* **4**, 46454 (2014).
- [35] T. Brächer, O. Boule, G. Gaudin, and P. Pirro, Creation of unidirectional spin-wave emitters by utilizing interfacial Dzyaloshinskii-Moriya interaction, *Phys. Rev. B* **95**, 064429 (2017).
- [36] A. Mook, J. Henk, and I. Mertig, Edge states in topological magnon insulators, *Phys. Rev. B* **90**, 024412 (2014).
- [37] X. S. Wang, Y. Su, and X. R. Wang, Topologically protected unidirectional edge spin waves and beam splitter, *Phys. Rev. B* **95**, 014435 (2017).
- [38] Z.-X. Li, Y. Cao, and P. Yan, Topological insulators and semimetals in classical magnetic systems, *Phys. Rep.* **915**, 1 (2021).
- [39] D. S. Han, A. Vogel, H. Jung, K. S. Lee, M. Weigand, H. Stoll, G. Schütz, P. Fischer, G. Meier, and S. K. Kim, Wave modes of collective vortex gyration in dipolar-coupled-dot-array magnonic crystals, *Sci. Rep.* **3**, 2262 (2013).
- [40] C. Behncke, M. Hänze, C. F. Adloff, M. Weigand, and G. Meier, Band structure engineering of two-dimensional magnonic vortex crystals, *Phys. Rev. B* **91**, 224417 (2015).
- [41] L. Sun, R. X. Cao, B. F. Miao, Z. Feng, B. You, D. Wu, W. Zhang, A. Hu, and H. F. Ding, Creating an artificial two-dimensional skyrmion crystal by nanopatterning, *Phys. Rev. Lett.* **110**, 167201 (2013).
- [42] A. Vansteenkiste, J. Leliaert, M. Dvornik, M. Helsen, F. Garcia-Sanchez, and B. V. Waeyenberge, The design and verification of MuMax3, *AIP Adv.* **4**, 107133 (2014).
- [43] A. A. Thiele, Steady-state motion of magnetic domains, *Phys. Rev. Lett.* **30**, 230 (1973).
- [44] W. P. Su, J. R. Schrieffer, and A. J. Heeger, Solitons in polyacetylene, *Phys. Rev. Lett.* **42**, 1698 (1979).
- [45] F. D. M. Haldane, Model for a quantum Hall effect without Landau levels: Condensed-matter realization of the “parity anomaly,” *Phys. Rev. Lett.* **61**, 2015 (1988).